J. of Fire Prot. Engr., 5 (2), 1993, pp 53-66

MODELING THE BURNER SOURCE USED IN THE ASTM ROOM FIRE TEST

by

Hao C. Tran[1]

USDA Forest Service
Forest Products Laboratory[2]
One Gifford Pinchot Drive
Madison, WI 53705-2398

Marc L. Janssens

American Forest & Paper Association
1250 Connecticut Avenue, NW
Washington, DC 20036

SUMMARY

Modeling fire growth over wall linings in a compartment requires experimental data and a model of the fire source. Limited information is available for flames against a wall or in a corner. Steady-state experiments were conducted to characterize the corner ignition source used in the proposed ASTM room fire standard at two heat release rate levels, 40 kW and 160 kW, with natural gas and a mixture of natural gas and toluene as the fuel. Flame height, heat flux to wall, temperature, velocity, mass and enthalpy flux, and flame structure were measured primarily in the flaming region. Correlation calculations included flame height as a function of heat release rate, and temperature, velocity, and mass flux for corner flames as a function of heat release rate and height.

INTRODUCTION

Fire growth on a wall and in the comer between two walls has been the subject of a joint study between the USDA Forest Service, Forest Products Laboratory (FPL) and the American Forest & Paper Association in the past few years[1-2]. The FPL room fire test facility has served two purposes: (a) to evaluate fire growth on wall linings, and (b) to develop and validate wall and corner fire models. The first purpose is fairly straightforward, while the second is complicated by factors involved in predicting fire growth, a major concern being the ignition source. In a sensitivity study, Tran and Janssens[1] examined the effect of burner setting on wood performance. In a subsequent study, a number of different wood products were tested using a burner program consisting of two steps: 40 kW for 5 min, followed by 160 kW for another 5 min[2]. Most wood products tested required 160 kW exposure to cause flashover, except for fire-retardant-treated wood, which did not result in flashover in these experiments.

To model the fire growth on the walls, the ignition source (burner) needs to be well characterized. While much work has been done on the structure and characteristics of axisymmetric flames and plumes[3-15], little

[1] Currently at USDA Forest Service, 14th and Independence SW, P.O. Box 96090, Washington, DC 20090-6090

[2] The Forest Products Laboratory is maintained in cooperation with the University of Wisconsin. This article was written and prepared by U.S. Government employees on official time, and it is therefore in the public domain and not subject to copyright.

information is available for flames and plumes that are constrained by the presence of walls[16-18]. We conducted steady-state experiments to obtain measurements to reconstruct the flame and plume physically, in a form suitable for modeling purposes. This paper focuses on characterizing the ignition source used in our room/corner fire tests and the resulting corner plume.

Generally, the terminology to describe a fire plume distinguishes between the combustion region and the plume above it. Turbulence causes the combustion region to oscillate between a continuous and an intermittent flaming region. The former is the region between the base of the burner and the maximum height below which a luminous flame is always observed. The latter is the region between the continuous flame tip and the minimum height where a flame is never observed, that is, the intermittent flame tip. Since we were interested only in heights smaller than the ASTM room height, most of our measurements were made in the flaming region. The resulting correlations are therefore valid for this region. Extrapolation of the equations into the overfire plume region, that is, beyond the maximum height at which measurements were made, has to be treated with caution.

EXPERIMENTAL

ASTM Burner

The ASTM proposed standard (1983) for room fire tests specifies that the burner be a square sand box, with the burning surface 0.305 m from the floor, and a square diffusion area of 0.305 by 0.305 m. The proposed standard does not specify the thickness of the burner box, but specifies that its edge be flush with the walls that form a corner. The FPL burner is made of 12.7 mm steel plate with outside dimensions of 0.330 by 0.330 m. In our experimental program, tests were conducted with the burner either against the back wall (wall tests) or in the comer of two walls (corner tests). We used C.P. grade propane (at least 99 percent pure) as specified by the proposed standard. The burner output in the proposed ASTM room standard was recently changed to 40 kW net heat release for 5 min followed by 160 kW for 10 min. This burner program was used in a worldwide round-robin exercise of the test method, and it is very likely to be adopted as an ASTM standard.

Experimental Design

To understand the transient nature of fire growth, it is necessary to understand the simpler steady-state scenario. From a practical point of view, steady-state experiments also provide ample time to obtain data, and instrumentation can be designed to thoroughly characterize the flame and fire plume.

The ASTM proposed standard prescribes C.P. grade propane for the gas burner. For our steady-state experiments, which lasted hours, the cost of C.P. grade propane was prohibitive. Natural gas was an attractive alternative because it is cheaper than propane and in abundant supply. However, natural gas is a much cleaner fuel than propane. To generate a flame that has more luminosity and soot, we used natural gas and a mixture of natural gas plus toluene to produce two levels of soot. Toluene was chosen for its relatively low boiling point and high soot formation propensity. The natural gas mixture contained approximately 90 percent methane and small fractions of ethane, propane, butane, approximately 0.5 percent CO_2, and 5 percent nitrogen plus argon. Natural gas flow was controlled via manual valves and monitored by a laminar flow device. The volumetric flow of gas was proportional to the pressure drop across the laminar flow device. Natural gas was available at supply pressure of 1,500 Pa. The pressure correction of 1.5 percent relative to atmospheric pressure was neglected. For the more sooty flames, toluene was metered in through a metering pump, vaporized, and blended with the incoming natural gas. Condensation was avoided by starting the toluene flow after preheating the burner to at least 60°C by burning natural gas. The ratio of natural gas to toluene was 9:1 based on net heat

release rate. The luminosity of propane is estimated to be somewhere between that of natural gas and the mixture.

Calcium silicate boards (marinite) were used for the walls because they are fairly durable (a thickness of 25 mm added strength), and their thermal properties are known.

Temperature, velocity, and species concentration profiles of the flame/plume were scanned in a two-dimensional horizontal grid at four different heights above the burner. The grid spacing was 25 mm. Some points were skipped toward the edge of the visible plume structure. The scanned areas and plane distance from burner are described in Table 1.

Table 1. Scanned areas and plane distance for flame/plume profiles

Flame	Total scanned area (m)	Plane distance from burner surface (m)
40 kW	0.305 by 0.305	0.305, 0.610, 0.915, 1.22
160 kW	0.356 by 0.356	0.305, 0.915, 1.525, 1.83

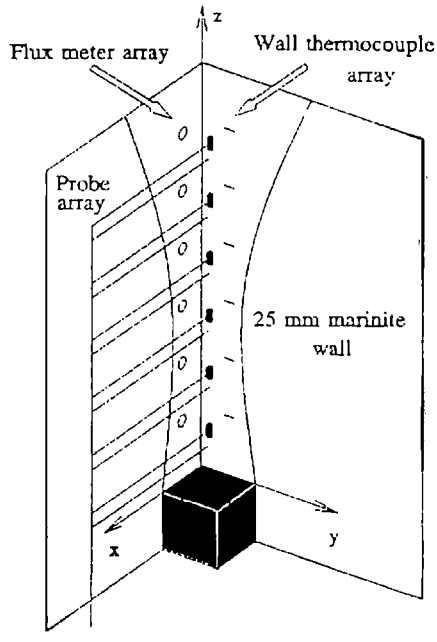

Figure 1—Experimental setup to characterize burner source in corner of two marinite walls.

Figure 1 shows the general construction of the corner walls and relative position of the instruments. Temperatures were obtained with a vertical array of four aspirated thermocouples, to scan the four selected planes. The aspirated thermocouples were constructed according to the design proposed by Newman and Croce[19]. In addition to measuring temperature, the aspirated thermocouples also served as gas sample probes. Gases were drawn from each probe through an arrangement of selecting valves to sample from one plane at a time. The sample stream, drawn from each probe through selecting valves, was filtered to remove soot and tar and scrubbed of water before being analyzed for oxygen, carbon monoxide, and carbon dioxide on a dry basis.

Velocity profiles of the flame and plume at selected heights were scanned by a vertical array of four bidirectional probes, made from 9.5-mm stainless steel barstock. The relatively small size of the probes was chosen to minimize intrusion into the flame. The bidirectional probes were arranged to be 25 mm ahead of the aspirated thermocouples to minimize the effect of aspiration on flow measurement. Differential pressures across the bidirectional probes were monitored by four separate transducers with a measuring range of 25 Pa.

Six total heat flux meters were mounted flush on one wall in a vertical array at increments of 0.305 m above the burner surface. The heat flux meter array was at a horizontal distance of 0.15 m from the corner. Similarly, the six pairs of thermocouples were at the same horizontal distance from the corner on the adjoining wall to measure the surface temperature and temperature drop across the wall.

Results

These experiments generated a massive amount of data; this report presents only data pertaining to the vertical structure of the flames and plumes and to some heat transfer aspects required specifically for modeling purposes.

Flame Height

Flame height was measured from photographic records of the flame taken at four frames per second. Flame tips (highest point) and continuous flame height were averaged over 36 exposures.

Because of the crude nature of flame height measurement, and as there is no apparent difference between the flame heights from the two fuel types, we used the data from the natural gas flames.

Table 2 lists the averages for the two heat release rates.

Table 2. Flame Height

Flame height (L_f) (m)

Fire Site	$\dot{Q}$ (kW)	Intermittent	Continuous	Mean	Reference
Open	40	0.78	0.40	0.59	17 (eqa. 2)
	160	1.60	0.82	1.21	17
Wall	40	0.92	0.58	0.75	17
	160	1.60	1.01	1.30	17
Corner	40	0.96	0.67	0.81	17
		0.80	0.60	0.70	FPL data
	160	2.41	1.68	2.04	17 (eqa. 2)
		1.97	1.61	1.79	FPL data

Hasemi and Tokunaga[17] correlated flame heights as a function of a characteristic heat release rate $\dot{Q}^*$:

$$\dot{Q}^* = \frac{\dot{Q}}{\rho_\infty c_p T_\infty g^{1/2} D^{5/2}} \qquad (1)$$

where D is the equivalent diameter of the source (m), $\dot{Q}$ is heat release rate (kW), and ρ_∞ and T_∞ are density (kg/m^3) and temperature (K) of ambient air, respectively.

Hasemi and Tokunaga[17] suggested that the heights of flames in an unconfined space, against a wall, and in a corner could be calculated as

$$L_f = D\gamma(\dot{Q}^*)^n \qquad (2)$$

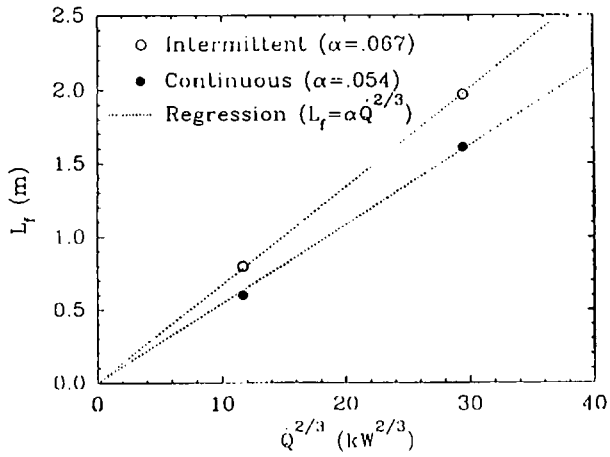

Figure 2—Corner flame height correlations.

where the value for n depends on the position of the flame, and the value for γ is different for continuous and intermittent flame heights. Table 3 lists values for n and γ for various flame types.

Table 3. Factors for calculating various flame types

Flame type	n for $\dot{Q}^*<1$	n for $\dot{Q}^*>1$	γ intermit.	γ contin.
Axisymmetric	2/3	2/5	3.5	1.8
Wall	**2/5**	**2/5**	**3.5**	**2.2**
Corner	**2/3**	**2/3**	**4.3**	**3.0**

The calculated flame heights according to Equation 2 for open flames, wall flames, and corner flames are listed in Table 2 together with flame heights from our experiments for comparison.

Corner flames are longer than wall flames and open flames in that order. This is consistent with observations made by Hasemi and Tokunaga.

For the ASTM corner burner, with a fixed D, Equation 2 becomes

$$L_f = \alpha(\dot{Q}^*)^n$$

with, according to Hasemi and Tokunaga[17], n=2/3 with α=0.089 and 0.062 for the intermittent and continuous flame heights, respectively. Figure 2 shows a similar power

law correlation of our flame height measurements. A value for n of 2/3 yielded good agreement, but resulted in values for α that were lower than those obtained by Hasemi and Tokunaga, that is, $\alpha = 0.067$ and 0.054 for the intermittent and continuous flame heights respectively. This clearly illustrates that our flame height measurements were lower. McCaffrey[3] used L_f to scale the height z in correlating flame and plume temperatures and velocities. Following the same idea with Equation 3, we used $z/\dot{Q}^{2/3}$ as the normalized height.

Heat Flux and Wall Surface Temperature

The average heat flux to the walls measured by the total heat flux meters is mapped in Figure 3 for the 40 and 160 kW corner flames. Figure 4 shows the steady-state surface temperatures of the fire-exposed side. Although one would expect a maximum flux and temperature close to the continuous flame tip, Figures 3 and 4 show that this is not the case. This is probably because all measurements were made at 0.15 m from the comer. The maximum at a given height may occur at another distance. In fact, the Gaussian plume profiles suggest maximum flux and temperature are likely to occur closer to the corner.

Figure 3—Heat flux to wall from corner flame and plume (0.15 m from corner). NG is natural gas, NGT natural gas plus toluene.

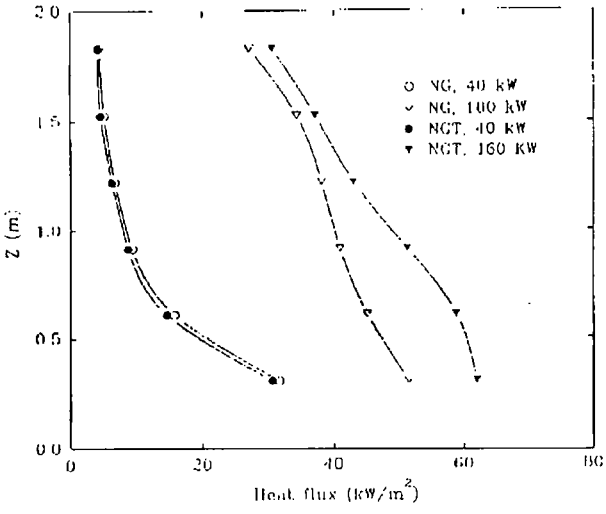

Mass Flow Calculations

Profiles of temperature, pressure drop across the velocity probes, and gas species concentration at different heights above the burner surface were obtained with the aspirated thermocouple and bidirectional probe assemblies. The procedure we used to calculate the mass flux is described as follows:

1. The combustion products, mostly CO_2 and H_2O, plus entrained air, are assumed to have the thermal properties of air. This assumption is usually made in fire plume studies in the absence of complete composition data and is usually adequate thanks to the dominant presence of N_2. Therefore, density can be calculated from the temperature data assuming the ideal gas law. The ideal gas law at constant pressure applied to air is

$$\rho = \frac{352.8}{T} \tag{4}$$

where ρ is the air density in kg/m^3, and T is the temperature in Kelvin.

2. The velocity profile is calculated based on pressure differential across the bidirectional probes and density calculated using assumption 1, according to

$$v = k\sqrt{\frac{2\Delta P}{\rho}} \tag{5}$$

Figure 4—Surface temperature of wall exposed to corner flame.

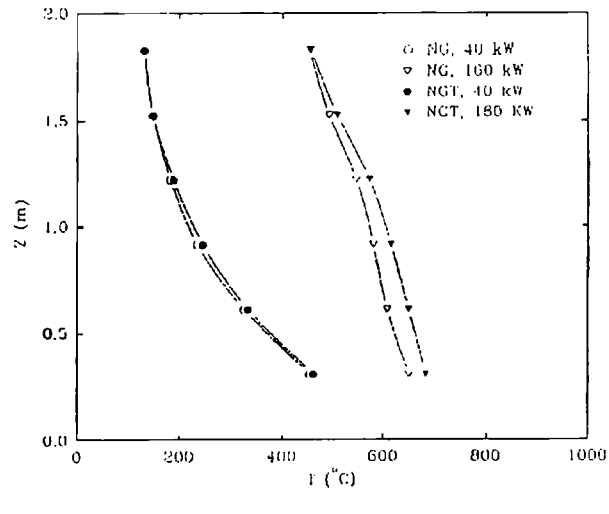

where k is the flow coefficient for bidirectional probes, and ΔP is the pressure drop across the probe (Pa).

3. Local mass flow is the product of velocity and density:

$$\dot{m} = v\rho \tag{6}$$

The data reduction procedure began with plotting the data in three-dimensional plots. Figure 5 shows an example of temperature profiles for a corner flame at one height. Figure 6 shows an example of contour topography of a temperature profile. The corner flames had their maxima very close to the corner. Although the actual temperature and velocity at the corner were not measured, to simplify the analysis, a maximum temperature of the profile was assumed to be at the corner. Despite some asymmetry, the contours were more or less concentric circles, so the profiles were about one-quarter of a conical profile. Our mathematical representation of the profiles were based on some techniques used by Kung and Stavrianidis[20] in modeling axisymmetric plumes.

Temperature Profile, Natural Gas, 40 kW Corner Flame
0.305 m above Burner

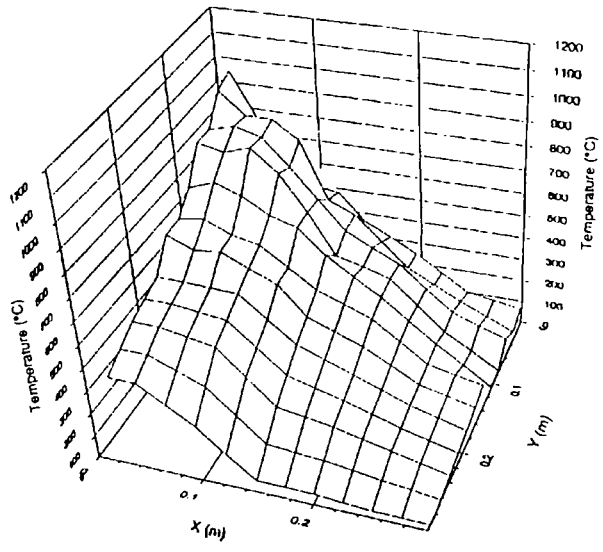

Figure 5—Temperature profile of 40 kW natural gas flame, 0.305 m above burner.

Temperature Contour, Natural Gas 40 kW Corner Flame
0.305 m above Burner

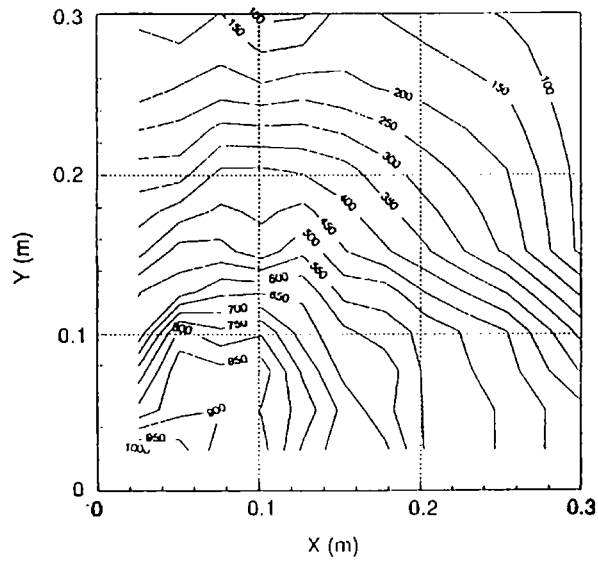

Figure 6—Temperature contour of 40 kW natural gas flame, 0.305 m above burner.

First, we reduced temperature to a dimensionless variable:

$$\Delta\overline{T} = \frac{\Delta T}{T_\infty} \tag{7}$$

where T_∞ (293 K) is the assumed ambient temperature and $\Delta T = T - T_\infty$.

$\Delta\overline{T}$ fit a Gaussian distribution of the form

$$\Delta\overline{T} = \Delta\overline{T}_c \exp\left(-\frac{(x-x_c)^2+(y-y_c)^2}{b^2}\right) \tag{8}$$

where $\Delta\overline{T}_c$ is the virtual maximum dimensionless temperature at the corner, x and y are the coordinates of the probe location, x_c and y_c are displacements of the maximum from the corner and are therefore zero, and b is the Gaussian half-width of the profile.

The velocity profile follows similarly:

$$v = v_c \exp\left(-\frac{x^2-y^2}{c^2}\right) \tag{9}$$

where v_c is the virtual velocity at the corner and c is the Gaussian half-width of the velocity profile.

Figures 7 and 8 show examples of the temperature and velocity profiles of one 40-kW

corner flame expressed as a function of radial distance r from the corner. Table 4 shows the values of $\Delta\overline{T}_c$ b, v_c, and c. Note that the values of b and c are almost identical for each height. This is different from the case of the axisymmetric flame structure, where b was reported by Kung and Stavrianidis[20] to be larger than c by a factor of 1.16.

Mass flux of the plume at a given height was obtained by numerical integration as follows:

$$\dot{m}_p = \frac{\pi}{2}\int_0^\infty \upsilon \rho r.dr \tag{10}$$

Using Equations 4 and 9, this becomes

$$\dot{m}_p = 1.891\int_0^\infty \frac{\upsilon_c \exp(-\frac{r^2}{c^2})}{\Delta\overline{T}_c \exp(-\frac{r^2}{b^2})+1} r.dr \tag{11}$$

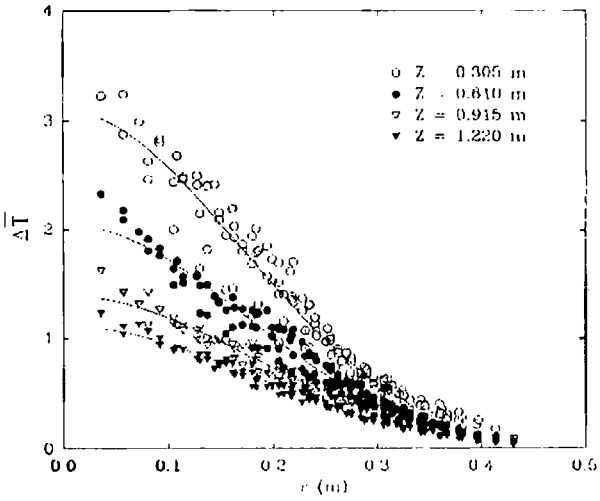

Figure 7—Gaussian temperature profiles of 40 kW natural gas flame at different heights.

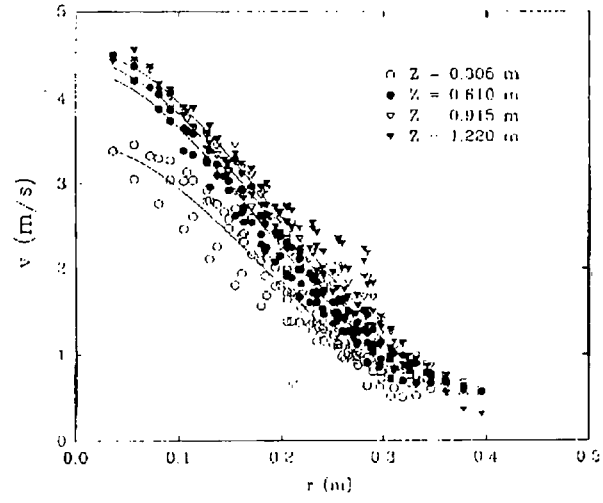

Figure 8—Gaussian velocity profiles of 40 kW natural gas flame at different heights.

Table 4. Characteristic temperature and velocity profiles

$\dot{Q}$ (kW)	Fuel type[a]	z (m)	$\Delta\overline{T}_c$	b (m)	υ_c (m/s)	c (m)
40	NG	0.305	3.176	0.249	3.934	0.268
		0.610	2.016	0.268	4.433	0.260
		0.915	1.339	0.283	4.441	0.268
		1.220	1.004	0.297	4.468	0.288
40	NGT	0.305	3.094	0.234	3.478	0.245
		0.610	2.055	0.237	4.321	0.246
		0.915	1.395	0.250	4.445	0.259
		1.220	1.116	0.251	4.557	0.266
160	NG	0.305	3.925	0.277	3.671	0.253
		0.915	3.274	0.339	6.400	0.317
		1.525	2.510	0.345	7.093	0.338
		1.830	2.276	0.335	7.164	0.348
160	NGT	0.305	3.945	0.263	3.754	0.264
		0.915	3.197	0.310	6.093	0.313
		1.525	2.515	0.325	6.803	0.338
		1.830	2.139	0.336	6.877	0.347

[a]NG is natural gas; NGT is natural gas plus toluene.

The calculated mass flux data are summarized in Table 5 and are plotted in Figure 9 as a function of height.

Enthalpy Flux

The enthalpy flux at each height was also calculated assuming that the combustion products had the properties of air:

$$\dot{Q}_c = \frac{\pi}{2}\int_0^\infty \rho h v r.dr \qquad (12)$$

with enthalpy defined as

$$h = C_p \Delta T \qquad (13)$$

with C_p= 1.017 kJ/kg•K. Using Equation 5, Equation 12 can be expanded to

$$\dot{Q}_c = 563.6\int_0^\infty \frac{\Delta\overline{T_c}\exp(-\frac{r^2}{b^2})}{\Delta\overline{T_c}\exp(-\frac{r^2}{b^2})+1} v_c \exp(-\frac{r^2}{c^2}) r.dr \qquad (14)$$

Figure 9—Mass flux of corner flame and plume.

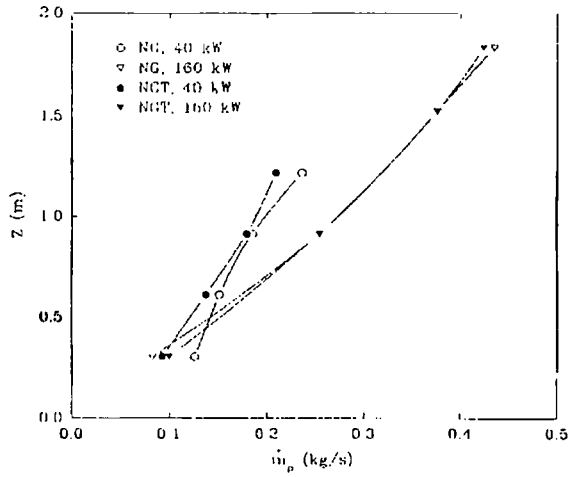

Figure 10—Enthalpy flux of corner flames and plume.

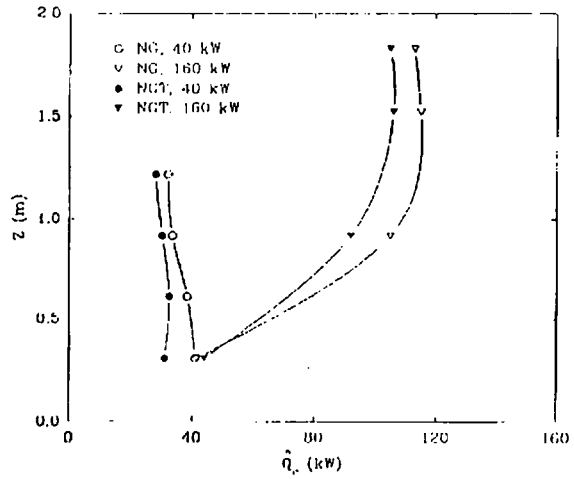

Table 5. Mass flux of fire plumes

$\dot{Q}$ (kW)	Fuel type	z (m)	$\dot{m}_p$ (kg/s)
40	NG	0.305	0.13
		0.610	0.15
		0.915	0.19
		1.220	0.24
40	NGT	0.305	0.09
		0.610	0.14
		0.915	0.18
		1.220	0.21
160	NG	0.305	0.08
		0.915	0.25
		1.525	0.38
		1.830	0.44
160	NGT	0.305	0.10
		0.915	0.25
		1.525	0.37
		1.830	0.42

Table 6 summarizes the calculated enthalpy flux data at different plume heights. Figure 10 plots the enthalpy flux data. As expected, the natural gas plumes were not as luminous as the natural gas and toluene mixture, resulting in smaller radiative losses and a higher enthalpy flux.

Table 6. Enthalpy flux of fire plumes

$\dot{Q}$ (kW)	Fuel type	z (m)	$\dot{Q}_c$ (kW)
40	NG	0.305	41
		0.610	38
		0.915	34
		1.220	32
40	NGT	0.305	31
		0.610	33
		0.915	30
		1.220	28
160	NG	0.305	42
		0.915	105
		1.525	115
		1.830	113
160	NGT	0.305	44
		0.915	92
		1.525	106
		1.830	105

Table 7.
Radiant heat flux from corner flames

$\dot{Q}$ (kW)	Fuel type	$\dot{q}''$ (kW / m^2) Radiometer 1	$\dot{q}''$ (kW / m^2) Radiometer 2
40	NG	1.42	2.91
	NGT	1.61	3.79
160	NG	7.44	7.46
	NGT	9.35	9.82

Emissive Power

To obtain some measure of the emissive power from the corner flames, two radiometers were used. They were water cooled and had a zinc sulfide window with a 90° view angle. Air was used to flush the windows to eliminate soot deposit. Meter 1 was placed 0.3 m from the burner center at the same height as the burner surface, facing up. Meter 2 was 0.9 m from the burner center, also at the same height as the burner surface, facing the flame. The two meters were placed on a line along an axis of symmetry of the corner burner setup (the principal diagonal). Table 7 summarizes the average radiant heat fluxes to these meters.

Again, the natural gas flames were less luminous than the flames of the fuel mixture, resulting in less radiative heat loss. The emissive power from the flames of the fuel mixture was 20–25 percent greater than that from the natural gas flames.

Discussion

This study was aimed at developing a model for flames in the confined space of the corner of two walls. Because we could not find any other detailed corner flame measurements, we cannot compare our experimental data directly with existing knowledge. However, as far as mass flux data are concerned, some room fire data for a corner burner can be used to check our results. Indeed, it is generally assumed in zone modeling that lower layer air entrainment is restricted to the vertical part of the flame and plume below the upper and lower layer interface. Therefore, if mixing between the layers is neglected, the mass outflow at the vent should equal the mass flux in the flame and plume at the interface height.

Using the classical plume theory of Morton et al.[14], Zukoski et al.[9] derived a mass flow formula that relates mass flux of an axisymmetric plume with heat release rate according to

$$\dot{m}_p \sim \dot{Q}^{1/3} \qquad (15)$$

Using this relationship, Mowrer and Williamson[18] argued that given the same $\dot{Q}$, a corner fire would develop 40 percent and a sidewall fire 63 percent of the mass flux of an axisymmetric fire in the center of a room. Since the excess temperature ($\Delta\overline{T}$) in the plume varies inversely with the mass flux (which is a function of air entrainment), the excess temperature of the corner plume and sidewall plume would be 2.5 and 1.6 times that of the center plume, respectively. However, these ratios are not exact in a room fire scenario because of the presence of an upper layer whose height varies with the source location. Mowrer and Williamson calculated layer height and mass flux of the plume, assuming no entrainment across the upper/lower layer interface based on a mass balance of the plume mass flux and doorway flow. They recommended mass flux ratios of 1.7 and 1.3 for center/corner and center/sidewall for a room fire facility similar to ours. Their calculations showed that for $\dot{Q}$ of 50 and 150 kW, the mass fluxes out the doorway were 0.48 and 0.60 kg/s for sidewall plumes and 0.35 and 0.45 kg/s for corner plumes, respectively.

Steckler et al.[21] placed a methane burner flush with the floor in a room 2.8 by 2.8 by 2.2 m, similar to the ASTM room, with a doorway 0.74 m wide and 1.83 m high. They measured inflow rates of 0.35, 0.45, and 0.50 kg/s for heat releases of 32, 63, and 105 kW, respectively. Using the fully-instrumented room test in the FPL room with gypsum wallboard lining and a new procedure to measure and calculate mass flow out the doorway, Janssens[22] calculated the doorway mass outflow of a propane corner fire to be 0.32 kg/s at 40 kW and 0.53 kg/s at 160 kW heat output. Janssens' data are quite consistent with the mass fluxes given by Mowrer and Williamson[18].

Visual observations and Janssens' calculations showed that the interface between the upper and lower layers in our room fires was located approximately 1.2 m above the burner surface. Our mass flux data at this height were 0.23 and 0.35 kg/s for the 40 and 160 kW flames, respectively. These values are lower than Janssens', because in an enclosure, some lower layer air entrained into the upper layer (presumably at the vent) accounts for part of the outflow[22].

These measurements appeared plausible enough to proceed to equations for reconstructing the plumes. A popular functional form to express the mass flux in terms of height and heat release rate is

$$\dot{m}_p = A\dot{Q}^m z^n \qquad (16)$$

where A is a constant embodying the entrainment coefficient, and m and n are constants reflecting the dependency on heat release rate and height, respectively. Equation 16 follows from the idea that at the flame tip, mass flux equals a certain multiple of the stoichiometric air required, independent of heat release rate. For example, correlations of axisymmetric flame and plume flow rates of the same form by McCaffrey[3] indicate that about 18 times the stoichiometric amount is entrained below the intermittent flame tip. Neglecting the mass flux of the fuel, this implies that m and n are interrelated. Taking into account that a nearly constant amount of air is needed for complete combustion of a mass unit of any fuel, substitution of Equation 3 into Equation 16 leads to the requirement that $m + 2/3n$ must be equal to 1. With this relationship in mind, we applied a curve fit to all mass flux data in Table 5 for the two levels of $\dot{Q}$, both fuel types, and all scanned heights. Introducing a constant into Equation 17 dramatically improved the agreement between predicted and measured $\dot{m}_p$. Figure 11 shows the result. The suggested correlation for mass flux is

$$\dot{m}_p = 0.062 + 0.042\dot{Q}^{0.27} z^{1.1} \qquad (17)$$

Figure 11—Agreement between calculated and measured mass fluxes.

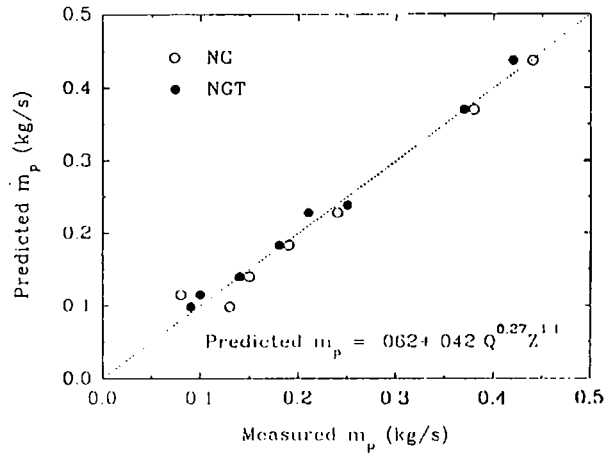

To predict centerline temperature and velocity, we attempted to use McCaffrey's approach[3]. Figures 12 and 13 show the results. Because of the limited number of measurements in the plume region, we grouped data points in the intermittent flame and plume regions together. The results of the correlations are as follows:

$$z < L_f \quad \text{or} \quad \frac{z}{\dot{Q}^{2/3}} < 0.054: \quad \Delta\overline{T_c} = 0.69\left(\frac{z}{\dot{Q}^{2/3}}\right)^{-2/5}$$

$$z > L_f \quad \text{or} \quad \frac{z}{\dot{Q}^{2/3}} > 0.054: \quad \Delta\overline{T_c} = 0.12\left(\frac{z}{\dot{Q}^{2/3}}\right)^{-1} \qquad (18)$$

and

$$z < L_f \quad \text{or} \quad \frac{z}{\dot{Q}^{2/3}} < 0.054: \quad \frac{v_c}{\dot{Q}^{1/3}} = 3.12\left(\frac{z}{\dot{Q}^{2/3}}\right)^{3/10}$$

$$z > L_f \quad \text{or} \quad \frac{z}{\dot{Q}^{2/3}} > 0.054: \quad \frac{v_c}{\dot{Q}^{1/3}} = 1.30 \qquad (19)$$

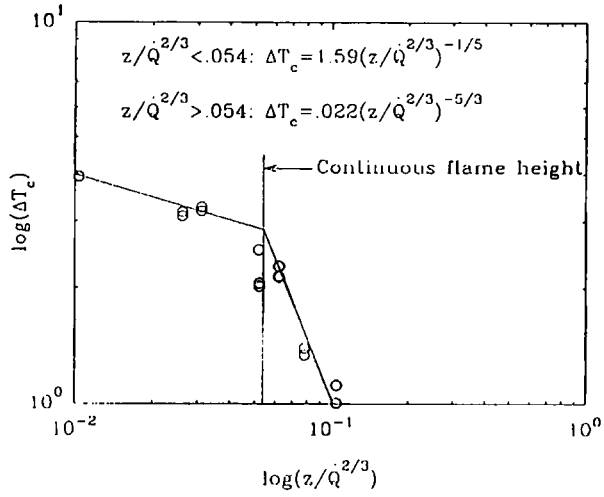

Figure 12—Correlation of centerline temperature with normalized height.

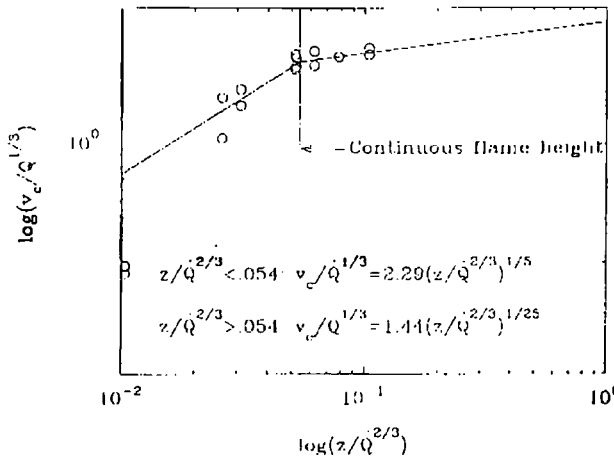

Figure 13—Correlation of centerline velocity with normalized height.

We expected a similarity between flames at different heat release levels. Following McCaffrey[3], we chose flame height to scale height z, leading to the normalized height parameter $z/\dot{Q}^{2/3}$. Centerline velocity is scaled on the basis of Bernoulli's theorem applied to a purely buoyant diffusion flame, neglecting wall friction:

$$\frac{1}{2}\rho v^2 \sim g\rho_\infty \frac{\Delta T}{T} z \qquad (20)$$

This leads to the definition of a buoyancy constant C:

$$\frac{v}{\sqrt{2g\frac{\Delta T}{T_\infty}z}} = C \qquad (21)$$

The value of C is approximately 0.85 over the whole range of heights at which we made our measurements, compared to 0.91 for axisymmetric flames and plumes obtained by McCaffrey[3]. Equation 18 indicates that $\Delta\overline{T_c}$ grows to infinity as z approaches zero. Obviously, this equation has to break down for small heights. We suggest using $\Delta\overline{T_c} = 4$ for $z/\dot{Q}^{2/3} < 0.012$. McCaffrey measured a constant $\Delta\overline{T_c} \approx 2.74$ over the whole continuous flame region of axisymmetric flames. Our $\Delta\overline{T_c}$ was higher because of the reduced air entrainment, and it dropped with height, presumably because of heat losses to the walls.

To reconstruct the corner plumes for the ASTM burner, we developed empirical equations that calculate the "centerline" temperature and velocity as functions of Q and z. The temperature and velocity profiles could then be found using the Gaussian forms introduced earlier in this report. The Gaussian half-widths were the last item needed to complete the picture. Another curve fit for the Gaussian half-width data (Table 4) was made with some good agreement between measured and calculated data on the curve fit (Figure 14). The proposed equation for both temperature and velocity Gaussian half-width is

$$b = c = 0.18\dot{Q}^{0.11} z^{0.12} \qquad (22)$$

An analysis of heat conduction across the wall or walls using surface temperature data and heat conductivity of the marinite materials showed that conduction loss was insignificant (1.5 kW/m^2 at most).

Convective heat flux data (Table 6) and radiative heat transfer to specific targets (Table 7) provide some feel for the radiative fractions. Table 6 shows that enthalpy flux is at a maximum near the continuous flame tip. Below the flame tip, there is excess unburnt fuel that has not been oxidized and released its chemical energy. In addition,

Figure 14—Agreement between calculated Gaussian half-widths for temperature and velocity profiles and measured values.

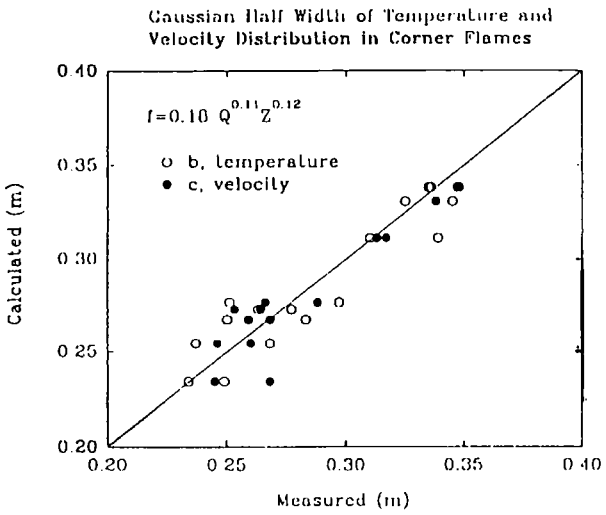

some heat is lost by radiation and convection to the walls and the surroundings. Above the flame tip, enthalpy flux decreases with height as a result of further losses. The difference between the chemical heat release rate ($\dot{Q}$), and the maximum enthalpy flux yields radiative losses from the luminous flames. The losses are 5 percent for the 40-kW natural gas, 18 percent for the 40-kW mixed fuel, 29 percent for the 160-kW natural gas, and 34 percent for the 160-kW mixed fuel flames. The radiative heat flux measurements in Table 7 support this analysis although calculating the heat flux to these flux meters requires significantly more analysis.

Conclusions

In this paper, we report some data obtained from steady-state experiments of gas burner flames. The reported data are restricted to the vertical part of the corner flames and plumes below turn at ceiling. Flame height correlations were somewhat lower than those of Hasemi and Tokunaga[17]. We found that the structure of a horizontal slice of the corner flame and plume could be represented as a quarter of a symmetric cone with the axis of symmetry having the maximum temperature and velocity located in the corner. The radial temperature and velocity profiles could be represented with simple Gaussian forms. We assumed that the thermal properties of the gas mixture were equal to those of air. Based on the temperature and velocity profiles, we derived mass flux and enthalpy flux of the flames and plumes by integration. Although there was a noticeable difference in radiation losses because of the fuel types used in these experiments, the temperature and velocity profiles of the plumes having the same $\dot{Q}$ were quite similar and can be generalized. Empirical equations that best fit the centerline temperature and velocity data and Gaussian half-widths have been proposed, in analogy with McCaffrey's equations for axisymmetric flames and plumes. Our correlations for $\Delta\overline{T}_c$ and v_c were not as accurate and detailed as those for axisymmetric flames and plumes in the literature. The great difficulty with which we obtained our data leaves us with admiration for others who did tedious work in this field, in particular the late Professor McCaffrey. Further measurements are needed to confirm or improve the correlations presented in this paper and to develop equations for the overfire plume region.

Nomenclature

A	constant
b	Gaussian half-width (m) of temperature profile
c	Gaussian half-width (m) of velocity profile
C	heat capacity ($Jkg^{-1}K^{-1}$)
D	diameter (m)
g	Gravitational constant (9.8 $m.s^{-2}$)
h	enthalpy (Jkg^{-1})
k	flow coefficient
L	length (m)
m	constant
$\dot{m}$	mass flow (kg/s)
n	constant
P	pressure (Pa)

$\dot{q}''$ heat flux (kW/m^2)

$\dot{Q}$ heat release rate (kW)

$\dot{Q}^*$ characteristic heat release rate (dimensionless)

r radial distance (m)

T temperature (K)

$\overline{T}$ dimensionless temperature

v velocity (m/s)

x coordinate (m)

Greek Symbols

α constant

γ constant

Δ difference

ρ density (kg/m^3)

Subscripts

∞ ambient

y coordinate (m)

z height (m)p plume

f flame

c centerline

References

1. Tran, H.C. and Janssens, M.L., "Room Fire Test for Fire Growth Modeling—A Sensitivity Study," *Journal of Fire Sciences.* **7**, 1989, pp. 217-236.
2. Tran, H.C. and Janssens, M.L., "Wall and Corner Fire Tests on Selected Wood Products," *Journal of Fire Sciences,* **9**, 1991, pp. 106-124.
3. McCaffrey, B.J., "Purely Buoyant Diffusion Flames: Some Experimental Results," U.S. Department of Commerce, Center for Fire Research, NBSIR 79-1910, 1979.
4. Delichatsios, M.A., "Air Entrainment into Buoyant Jet Flames and Pool Fires," *SFPE Handbook of Fire Protection Engineering,* Dinenno, P.J., ed., National Fire Protection Association, Section 1, Chapter 19, 1988.
5. Tokunaga, T., Sakai, T., Kawagoe, K., Tanaka T., and Hasemi, Y., "Mass Flow Rate Formula for the Upward Current above Diffusion Flames," *Fire Science and Technology,* **2**, No. 2, 1982, pp. 117-125.
6. Schneider, M.E. and Kent, L.A., "Measurements of Gas Velocities and Temperatures in a Large Open Pool Fire," *Fire Technology,* **25**, No. 1, 1989, pp. 51-78.
7. Jeng, S-M., Lai, M-C., and Faeth, G.M., "An Investigation of Axisymmetric Buoyant Turbulent Diffusion Flames: Flow Structure and Radiation Properties," U.S. Department of Commerce, Center for Fire Research, NBS-GCR-84-458, 1984.
8. Jeng, S-M., Chen, L.D., and Faeth, G.M., "An Investigation of Axisymmetric Buoyant Turbulent Diffusion Flames: Turbulence Properties and Concentrations of Major Species," U.S. Department of Commerce, Center for Fire Research, NBS-GCR-83-422, 1983.
9. Zukoski, E.E., Kubota, T., and Cetegen, B., "Entrainment in Fire Plumes," *Fire Safety Journal,* 3, 1980/81, pp. 107-121.
10. Toner, S.J., Zukoski, E.E., and Kubota, T., "Entrainment, Chemistry, and Structure of Fire Plumes," U.S. Department of Commerce, Center for Fire Research, NBS-GCR-87-528, 1987.
11. Heskestad, G., "Virtual Origins of Fire Plumes," *Fire Safety Journal,* **5**, 1983, pp. 109-114.
12. Fang, J.B., "Analysis of the Behavior of a Freely Burning Fire in a Quiescent Atmosphere," U.S. Department of Commerce, Center for Building Technology, NBSIR 73-115, 1973.
13. Morton, B.R., "Modeling Fire Plumes," 10th International Symposium on Combustion, Pittsburgh, PA: The Combustion Institute, 1965, pp. 973-982.
14. Morton, B.R., Taylor, Sir G., and Turner, J.S., "Turbulent Gravitational Convection from Maintained and Instantaneous

Sources," Proceedings of the Royal Society of London, Vol. **234**, Series A, No. 1196, 1956.
15. Cox, G. and Chitty, R., "A Study of the Deterministic Properties of Unbounded Fire Plumes," *Combustion and Flame,* **39**, 1980, pp. 191-209.
16. Lai, M.C. and Faeth, G.M., "The Structures of Adiabatic Wall Plumes," U.S. Department of Commerce, Center for Fire Research, NBS Grant Number 60NANB4D0032, 1985.
17. Hasemi, Y. and Tokunaga T., "Some Experimental Aspects of Turbulent Diffusion Flames and Buoyant Plumes from Fire Sources against a Wall and in a Corner of Walls," *Combustion Scienceand Technology*, **40**, 1984, pp. 1-17.
18. Mowrer, F.W. and Williamson, R.B., "Estimating Room Temperatures from Fires along Walls and in Corners," *Fire Technology,* **23**, 1987, pp. 133-145.
19. Newman, J.S. and Croce, P.A., "A Simple Aspirated Thermocouple for Use in Fires," *Journal of Fire and Flammability*, **10**, 1979, pp. 326-336.
20. Kung, H-C. and, Stavrianidis, P., "Buoyant Plumes of Large-Scale Pool Fires," 19th International Symposium on Combustion, Pittsburgh, PA., The Combustion Institute, 1982, pp. 905-912.
21. Steckler, K.D., Quintiere, J.G., and Rinkinen, W.J., "Flow Induced by Fire in a Compartment," U.S. Department of Commerce, Center for Fire Research, NBSIR 82- 2520, 1982.
22. Janssens, M.J., Ph.D. Dissertation, University of Gent (Belgium), 1991.